Supplementary Information

Quantitative Distribution Model of Dendrites in Li metal batteries

Guanwu Li, Chichu Qin, Dong Wang*, Yumin Liu, Hengguang Zhang, Yingpeng Wu*

State Key Laboratory of Chem/Bio-Sensing and Chemometrics, College of Chemistry and Chemical Engineering, Hunan University, Changsha 410082, P. R. China.

*Corresponding Author

E-mail addresses: wuyingpeng@hnu.edu.cn (Y. P. Wu),

wangdong14@hnu.edu.cn (D. Wang)

Supplemental Figures and Supplemental Tables.

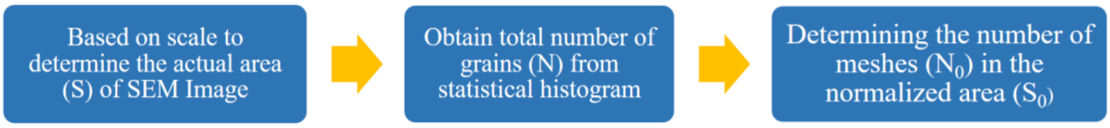

Supplementary Fig. 1 The process of divided mesh according to the histogram. Here $N_0 = \frac{N * S_0}{S}$, where S is actual area (S) of SEM Image, N is total number of grains and S_0 is the normalized area that is $1mm^2$.

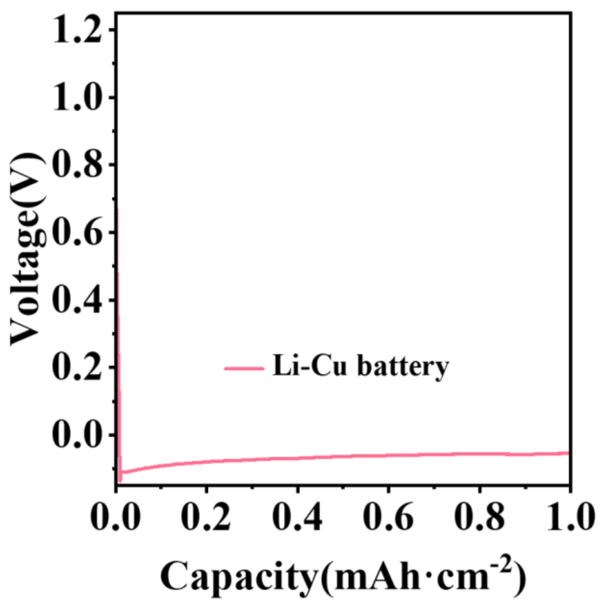

Supplementary Fig. 2 Capacity-voltage curve for Li/Cu battery at 1 mAh cm^{-2} and 1 mA cm^{-2}. As the capacity-voltage curve of Li/Cu battery shown (Supplementary Fig. 2), the process of Li platting onto the copper surface is divided into two stages as nucleation and growth. On proof of our concept, different distribution states in gradient entropies were realized as a fixed mol (4 mAh cm^{-2}) of lithium deposited onto the Cu foil by using Swagelok battery (Supplementary Fig. 3A). Thus, we divide the total mol (4 mAh·cm^{-2}) of deposited lithium into nucleation mol (0.2 mAh·cm^{-2}, at four types of 0.1, 0.5, 1, 10 mA·cm^{-2}, named as $Li_{0.1M}$, $Li_{0.5M}$, $Li_{1.0M}$, Li_{10M}, respectively) and growth mol (3.8 mAh·cm^{-2}, at 1 mA·cm^{-2}). Notably, the jump in the time voltage curve is related to nucleation overpotential and the change of current (Supplementary Fig. 4). Based on these four anodes, CR2032 cells were assembling, diagrammatic in Supplementary Fig. 3B, Supplementary Fig. 3C.

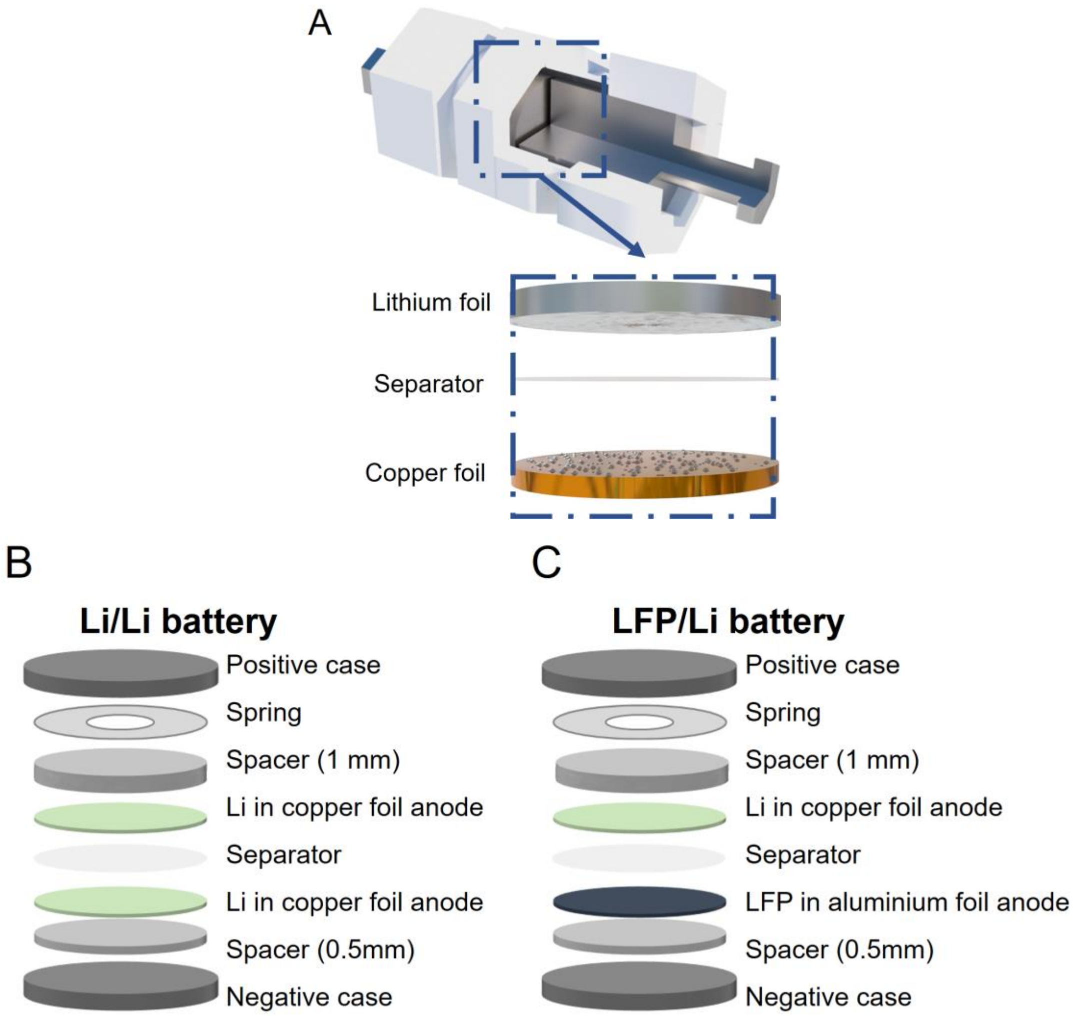

Supplementary Fig. 3 Schematic diagram of the battery used for the test in this article. (A) Schematic diagram of the structure of the Swagelok battery and Schematic diagram of the structure for the Li/Li battery (B) and LFP/Li battery (C).

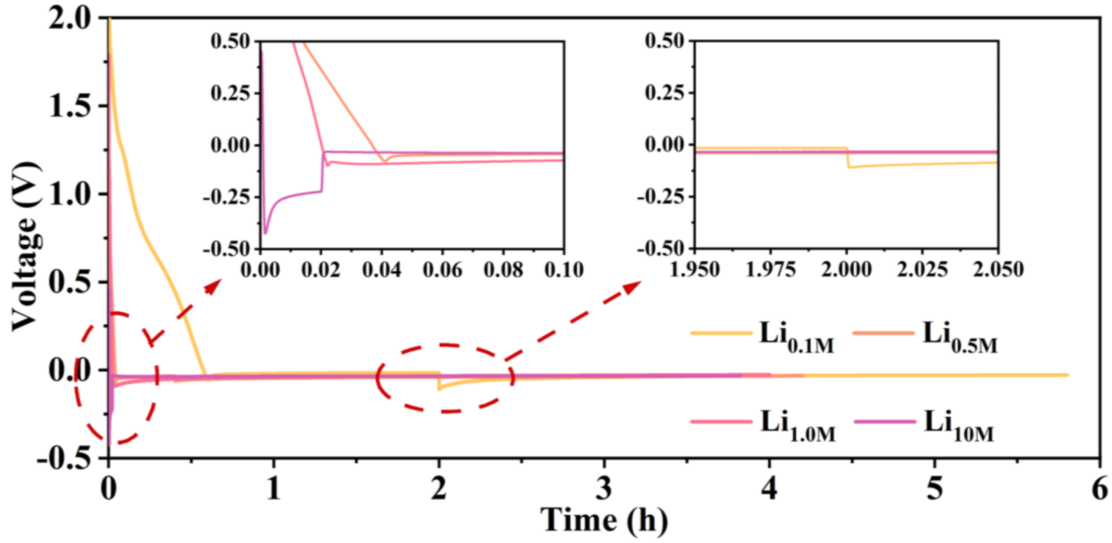

Supplementary Fig. 4 Time voltage curve of the Swagelok battery for acquiring these four anodes. Four lines represent four samples ($Li_{0.1M}$, $Li_{0.5M}$, $Li_{1.0M}$ and Li_{10M}) respectively.

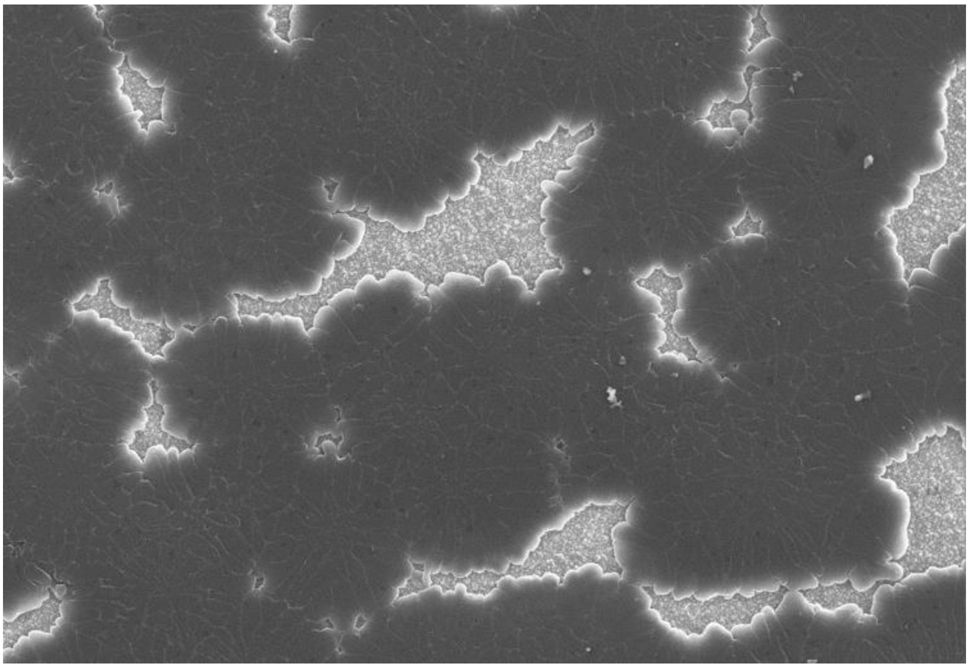

Supplementary Fig. 5 SEM images of $Li_{0.1M}$ at 200 times. The image shows $Li_{0.1M}$ has the largest crystal nucleus in these four samples.

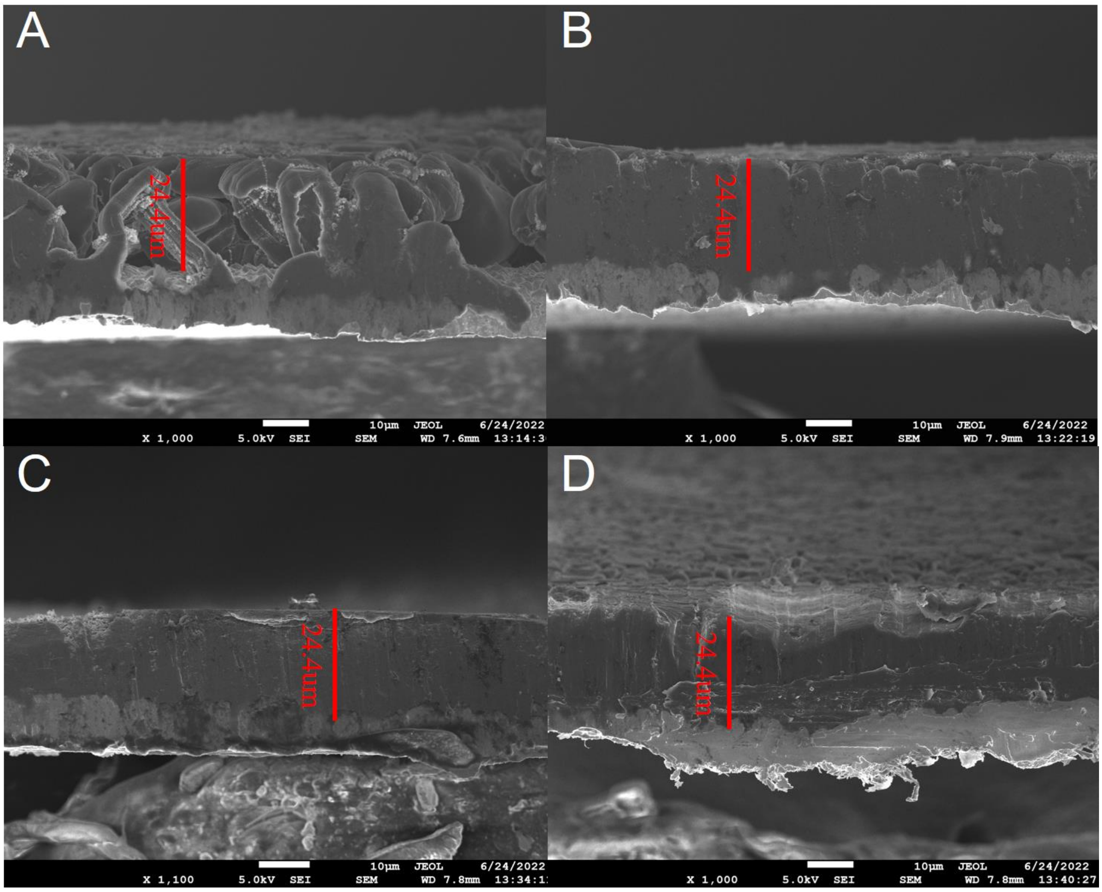

Supplementary Fig. 6 Cross section SEM images of (A) $Li_{0.1M}$, (B) $Li_{0.5M}$, (C) Li_{1M}, (D)Li_{10M}. These images show these four anodes have almost same height.

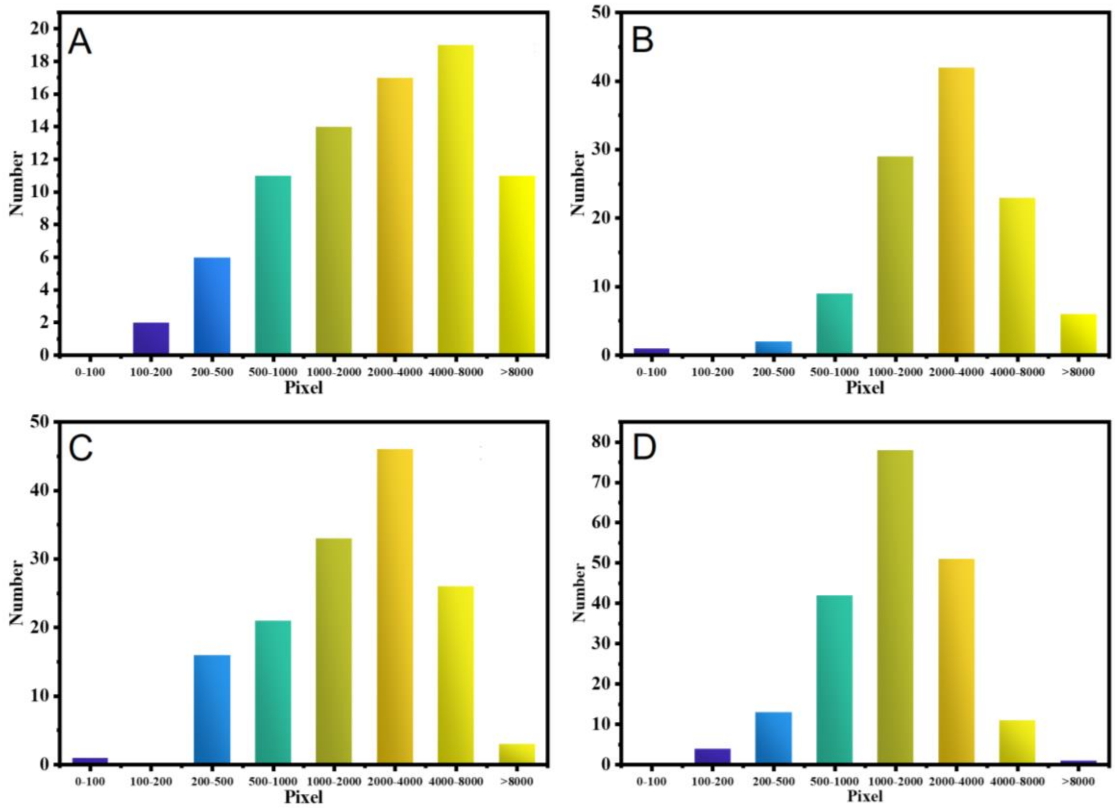

Supplementary Fig. 7 Grain statistical information. According to the SEM images for these four anodes, Grain statistical information of $Li_{0.1M}$ (A), $Li_{0.5M}$ (B), $Li_{1.0M}$ (C) and Li_{10M} (D) were acquired.

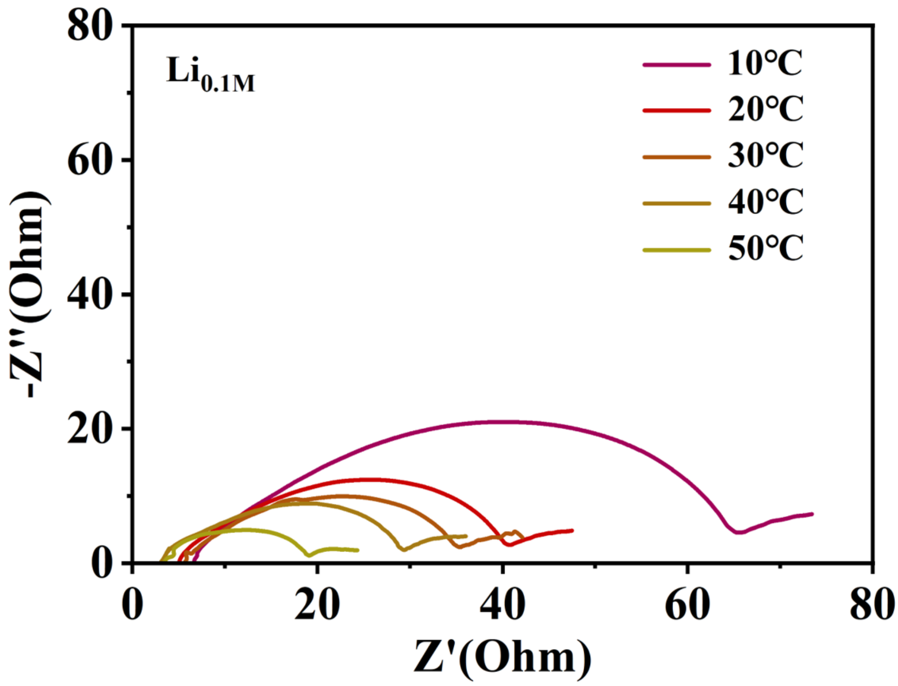

Supplementary Fig. 8 EIS curve for $Li_{0.1M}$ / $Li_{0.1M}$. It was measured at different temperatures and shows in five lines.

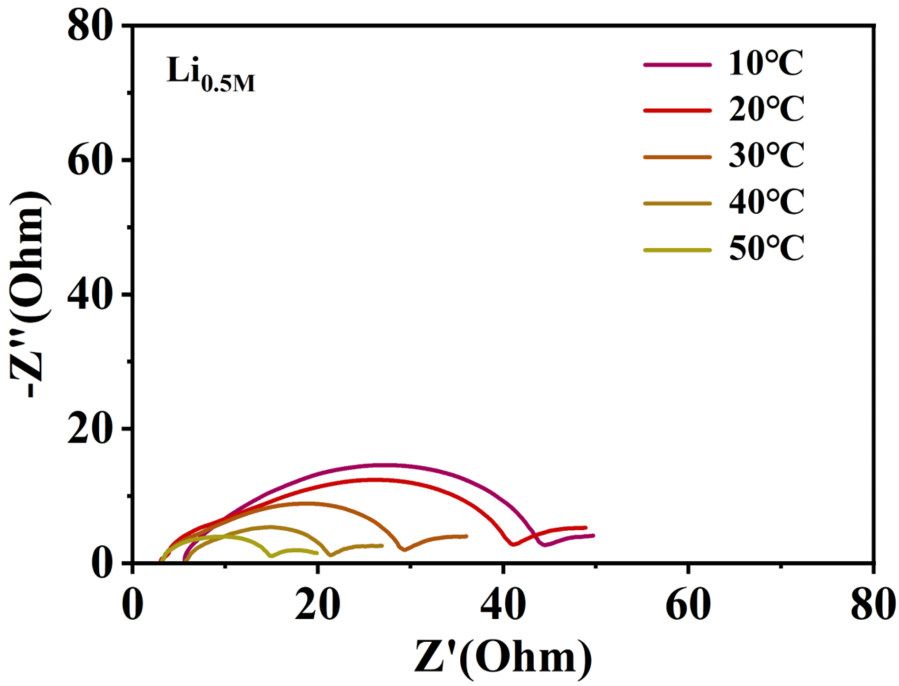

Supplementary Fig. 9 EIS curve for Li$_{0.5M}$ / Li$_{0.5M}$. It was measured at different temperatures and shows in five lines.

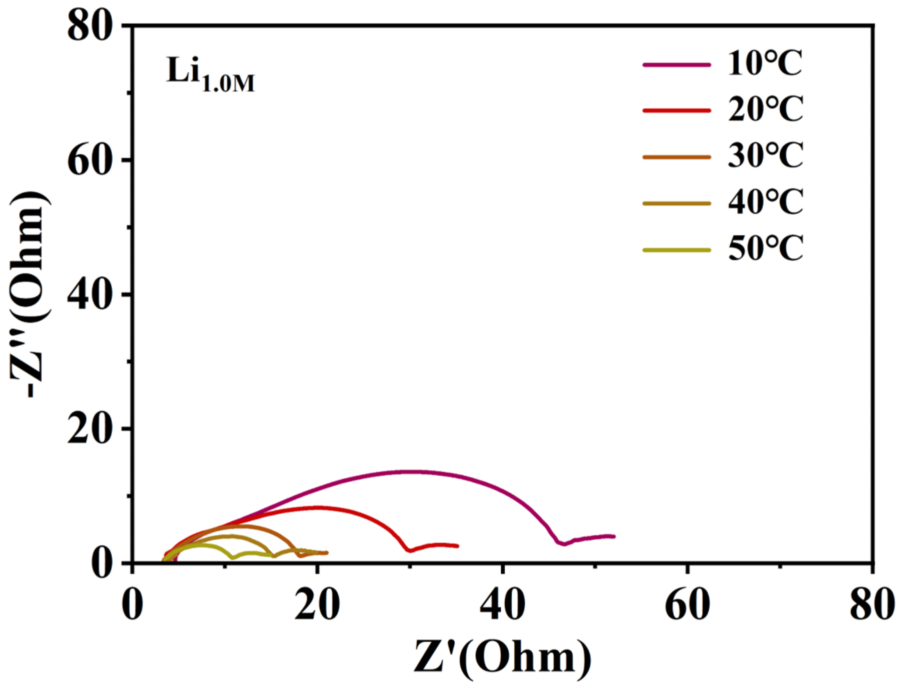

Supplementary Fig. 10 EIS curve for $Li_{1.0M}$ / $Li_{1.0M}$. It was measured at different temperatures and shows in five lines.

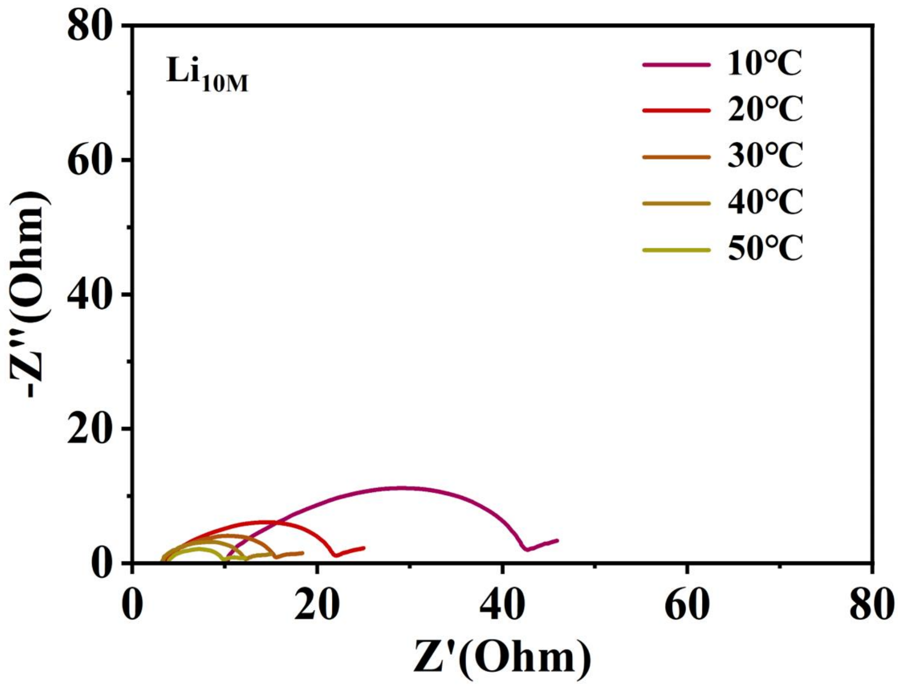

Supplementary Fig. 11 EIS curve for Li_{10M} / Li_{10M}. It was measured at different temperatures and shows in five lines.

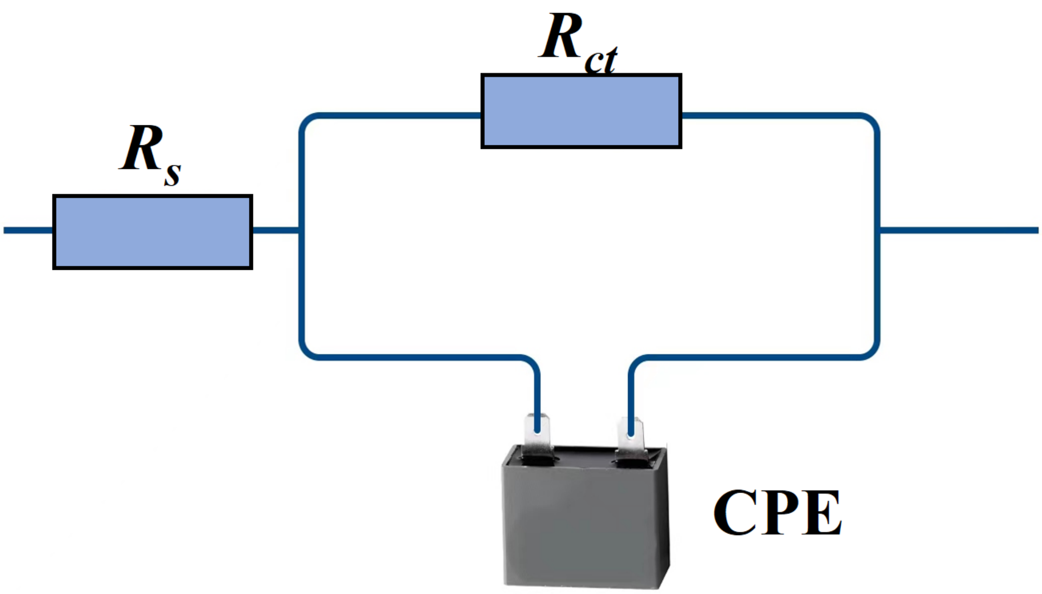

Supplementary Fig. 12 The equivalent circuit diagram of fitting the EIS results of all symmetrical batteries in different temperature. For this equivalent circuit diagram, the EIS results can be well fitted by using it, where R_s is the ohm resistance about all symmetrical batteries, R_{ct} represents the charge-transfer resistance generated at interfaces and CPE means constant phase element.

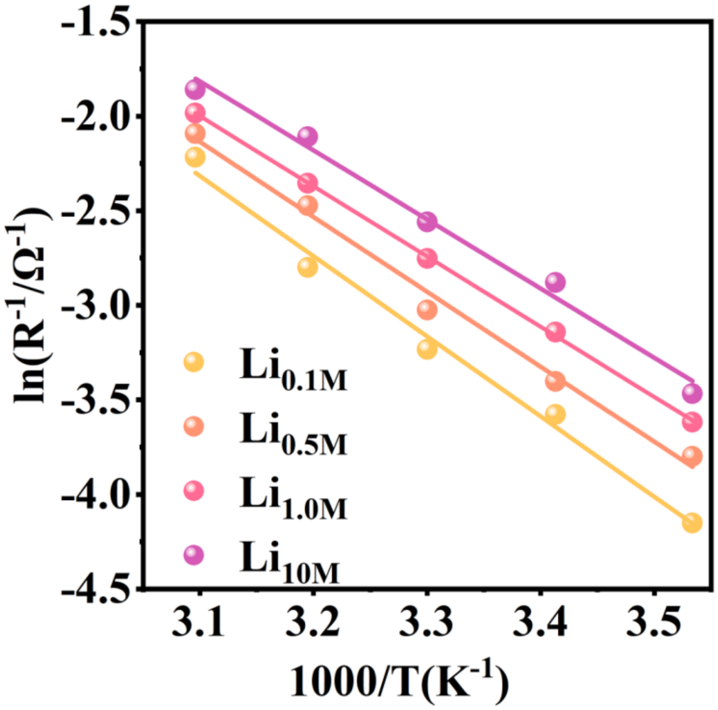

Supplementary Fig. 13 Straight line fitted by R_{ct} from EIS. Corresponding comparison of activation energies was got from symmetrical battery for $Li_{0.1M}$, $Li_{0.5M}$, Li_{1M} and Li_{10M}.

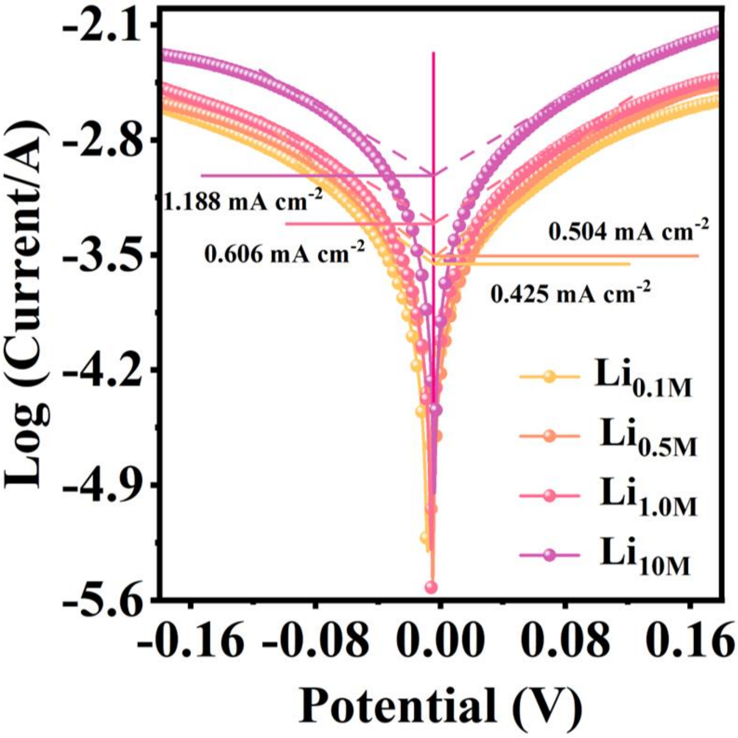

Supplementary Fig. 14 Tafel curve for these four anodes. Tafel slope and exchange current density obtained from this curve of Li/Li battery for $Li_{0.1M}$, $Li_{0.5M}$, Li_{1M} and Li_{10M} after first cycle

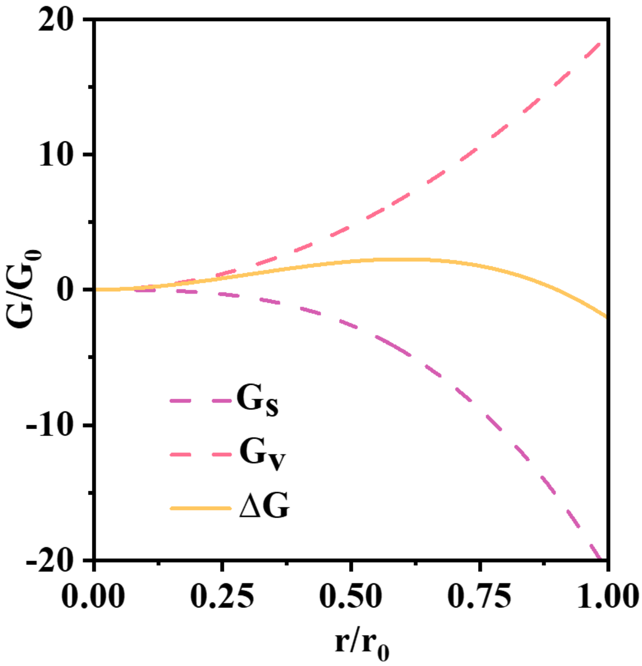

Supplementary Fig. 15 Laplace equation curve. This curve was inferred from Laplace equation include system nucleation Gibbs free energy, G_s interface energy, G_v bulk energy, ΔG nucleation drive energy.

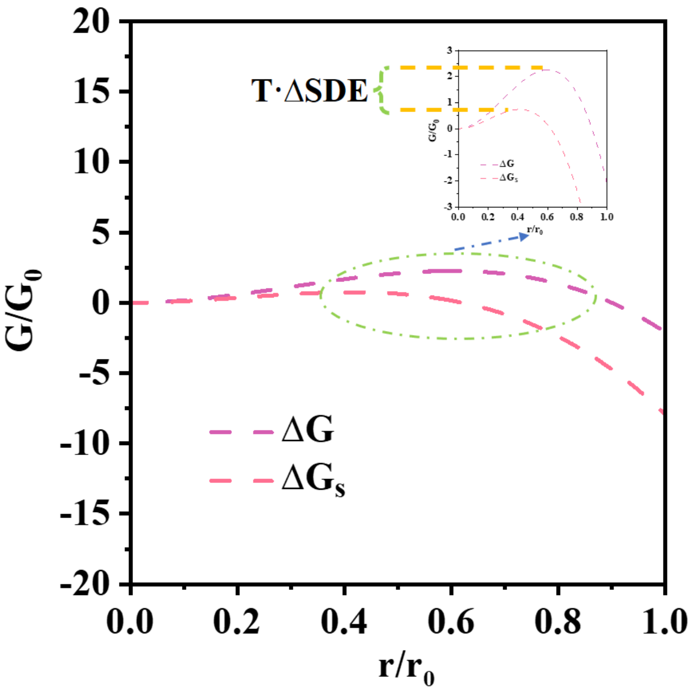

Supplementary Fig. 16 Laplace equation curve coupled with SDE. This curve shows system nucleation driving energy ΔG and it coupling of SDE is ΔG_s.

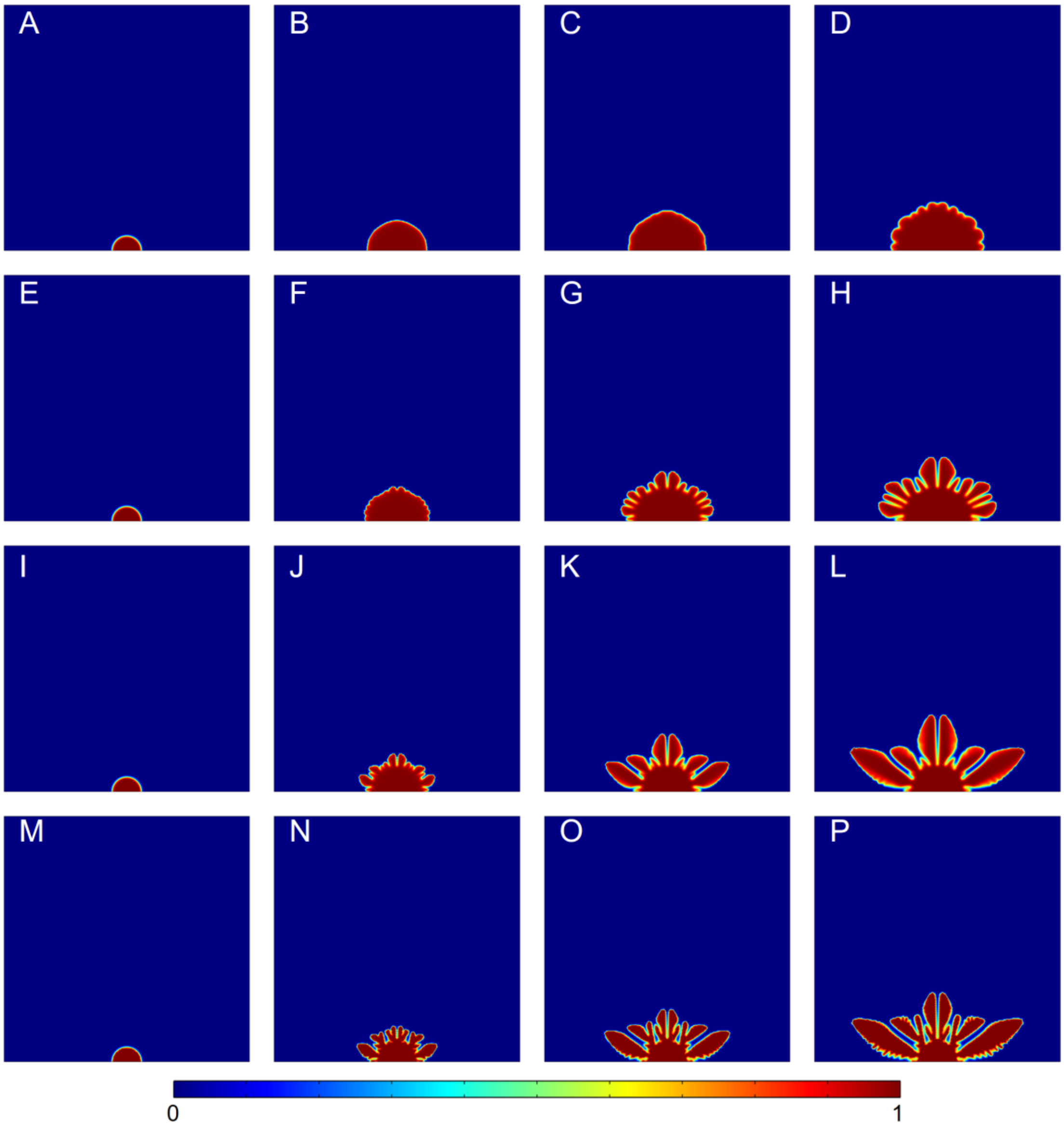

Supplementary Fig. 17 Result of MPFCS model for $\xi(r, t)$. These show $\xi(r, t)$ of Li_{10M} (A-D), $Li_{1.0M}$ (E-H), $Li_{0.5M}$ (I-L) and $Li_{0.1M}$ (M-P) at 0, $t_0/3$, $2t_0/3$ and t_0.

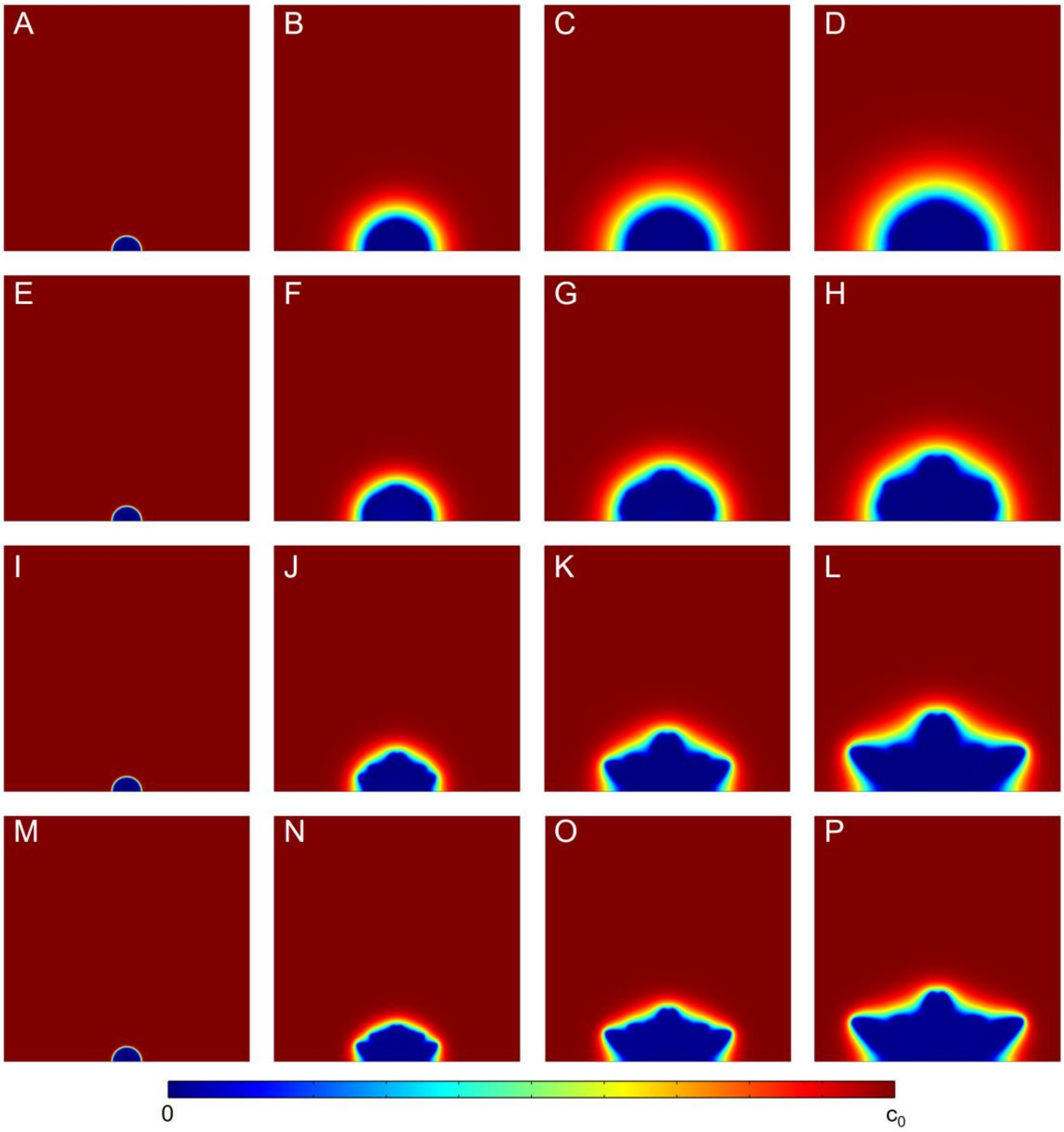

Supplementary Fig. 18 Result of MPFCS model for $c(r,t)$. These show $c(r,t)$ of Li_{10M} (A-D), $Li_{1.0M}$ (E-H), $Li_{0.5M}$ (I-L) and $Li_{0.1M}$ (M-P) at 0, $t_0/3$, $2t_0/3$ and t_0.

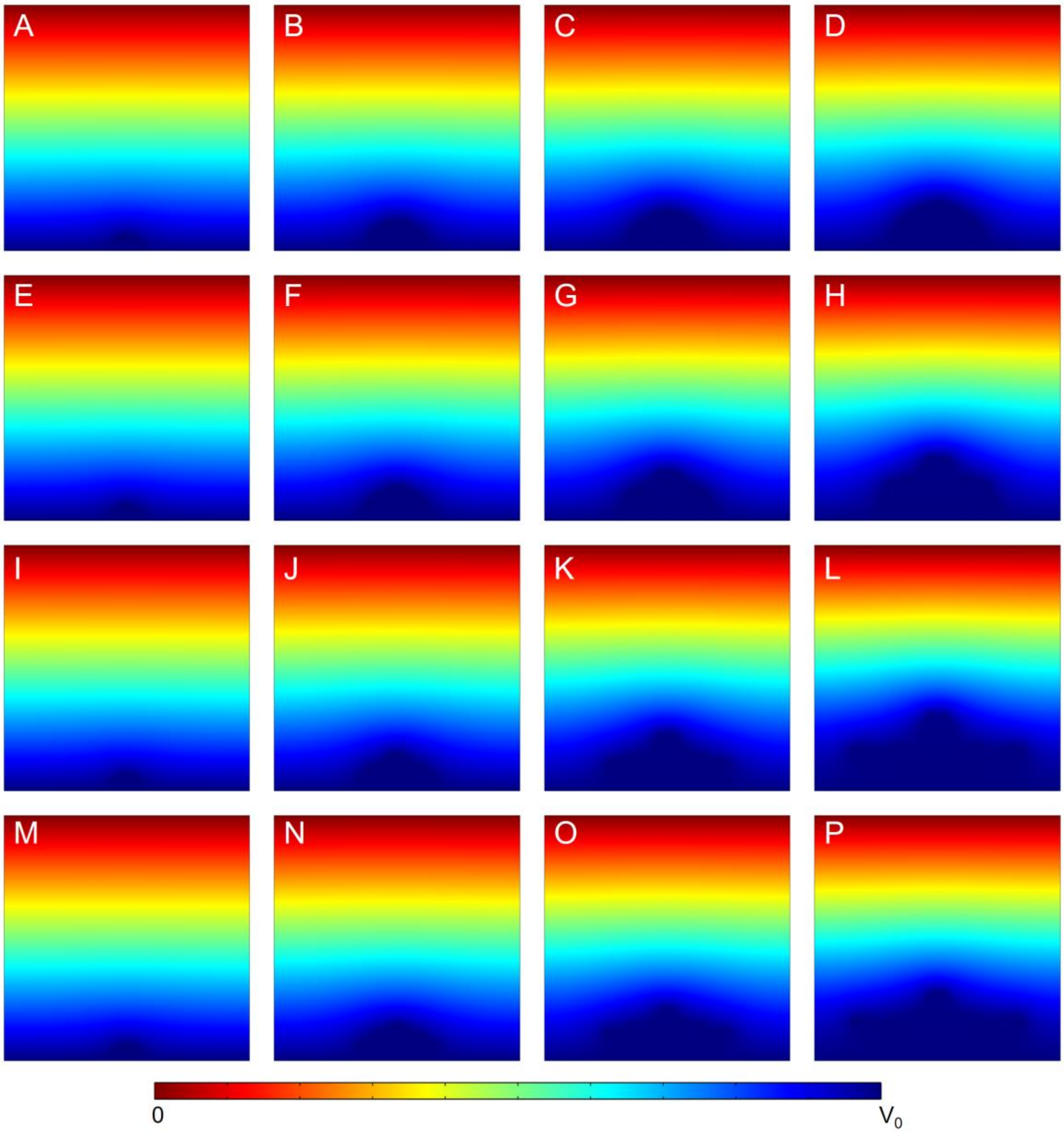

Supplementary Fig. 19 Result of MPFCS model for $\phi(r,t)$. These show $\phi(r,t)$ of Li_{10M} (A-D), $Li_{1.0M}$ (E-H), $Li_{0.5M}$ (I-L) and $Li_{0.1M}$ (M-P) at 0, $t_0/3$, $2t_0/3$ and t_0.

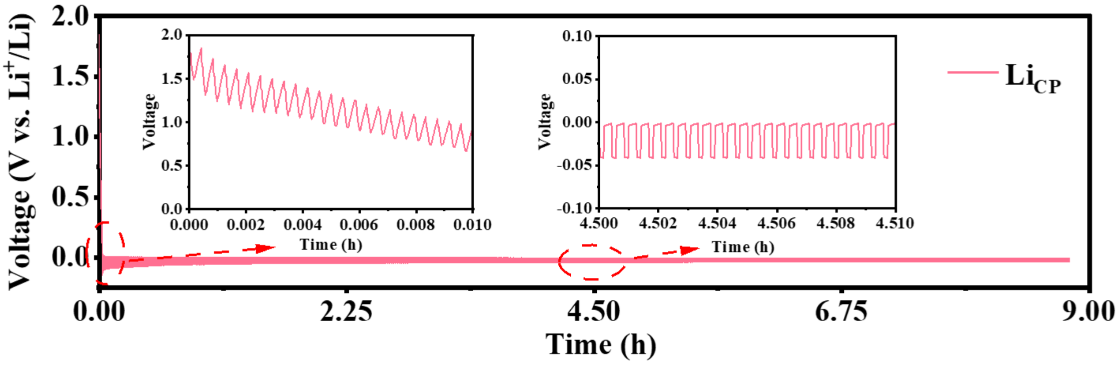

Supplementary Fig. 20 Time-Voltage curve for Swagelok battery of Li/Cu by using the charging protocol. This curve shows the voltage information that changes with the current.

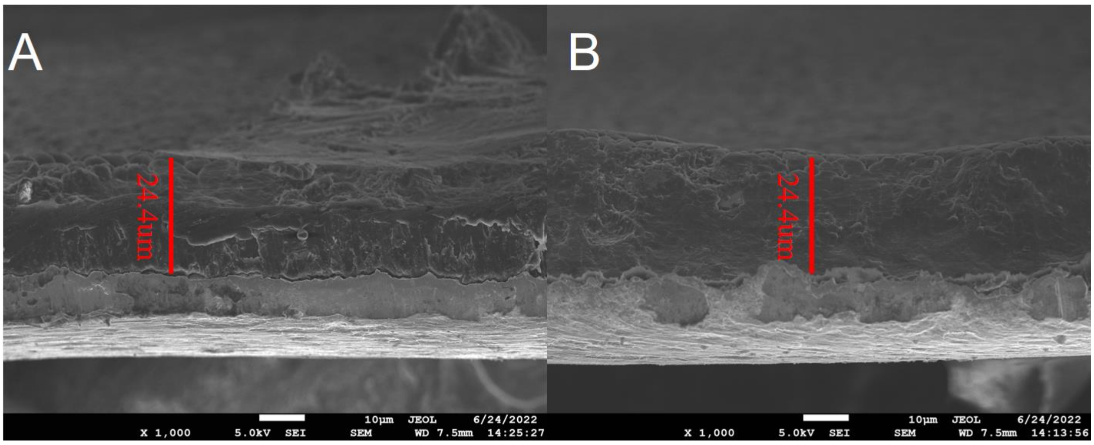

Supplementary Fig. 21 Cross section SEM images of Li_{CP} (A) and Li_{CPA} (B). These cross-section images for Li_{CP} and Li_{CPA} show that the thickness of the lithium cross-section is almost unchanged, indicating that these two methods can successfully make grain tinier without changing the amount of lithium deposition.

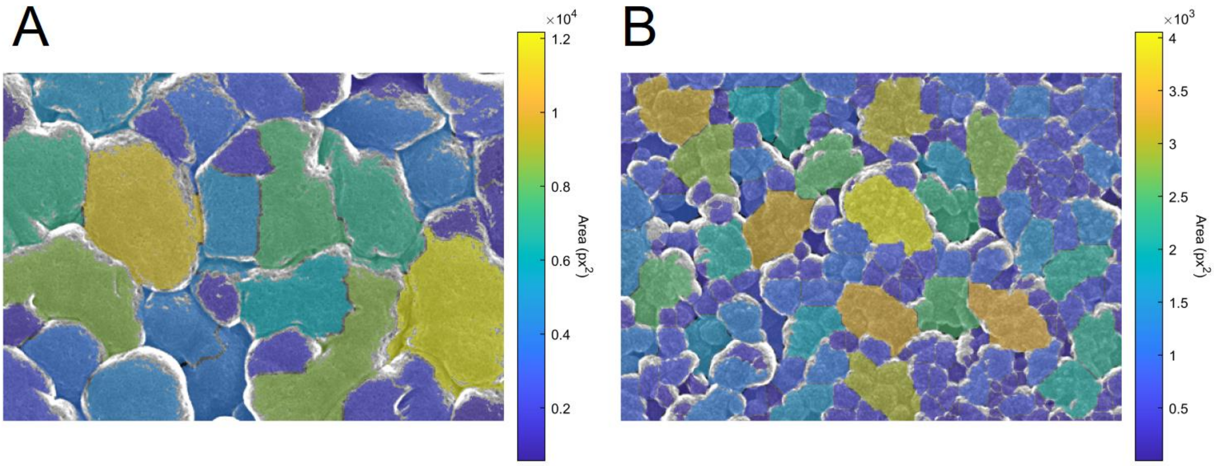

Supplementary Fig. 22 Crystal division images of Li_{CP} (A)and Li_{CPA} (B). These images are obtained by the method in manuscript section 1 according to SEM images.

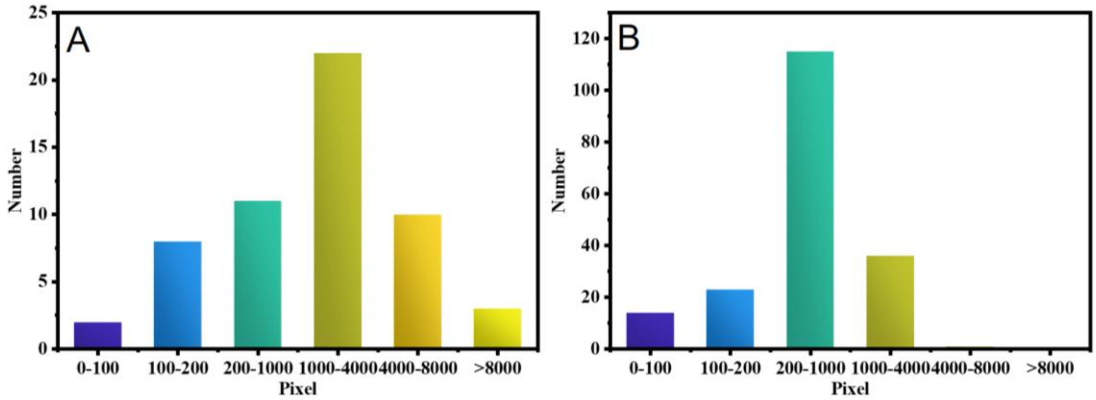

Supplementary Fig. 23 Grain statistical information. According to the SEM images for these four anodes, Grain statistical information of Li_{CP} (A) and Li_{CPA} (B).

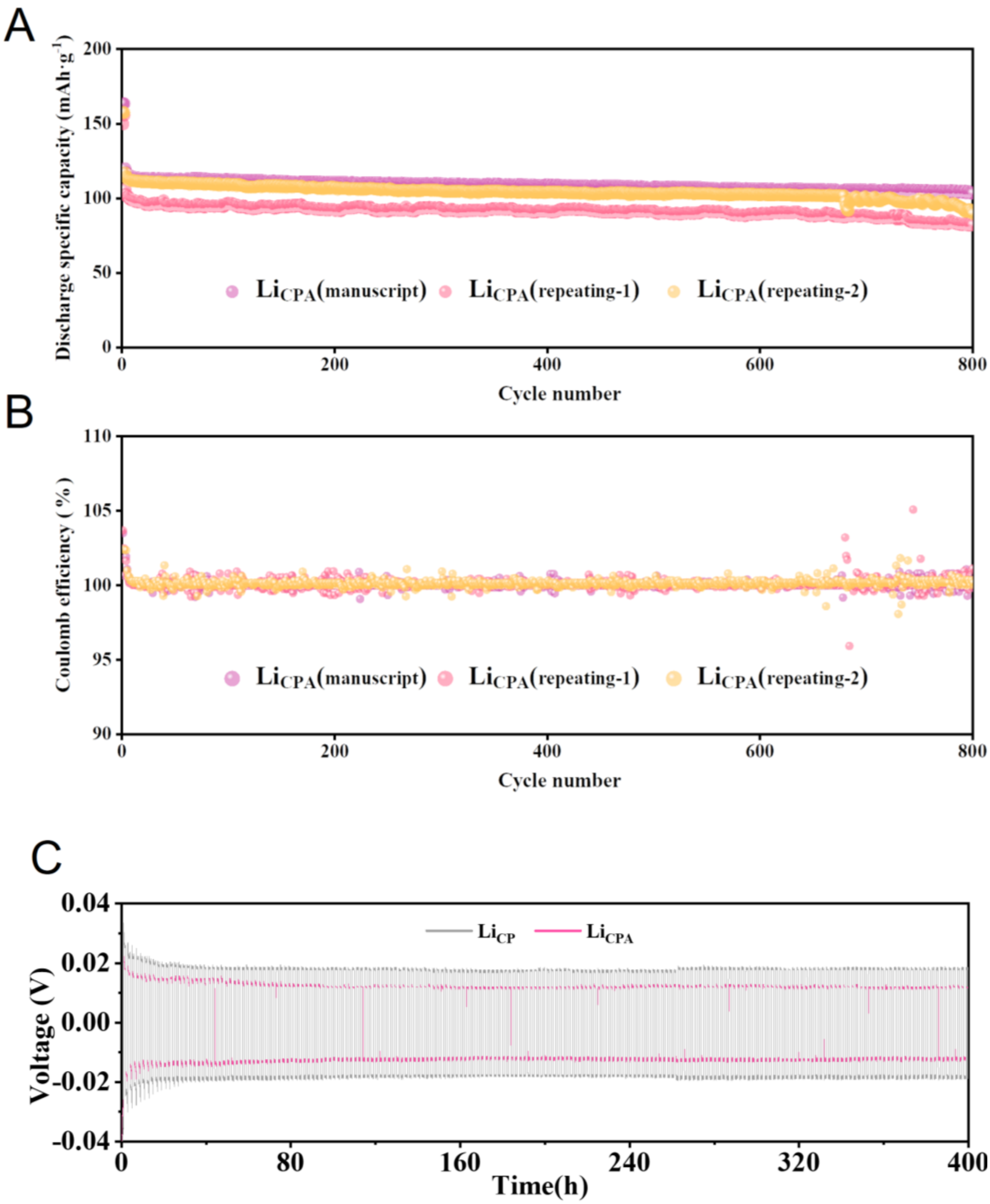

Supplementary Fig. 24 Repeating data for Li_{CPA}/LFP. (A) Capacity curve and (B) Coulomb efficiency curve. (C)Time-voltage curves of Li/Li battery for Li_{CP} and Li_{CPA} in 1mA • cm^{-2} and 1 mAh • cm^{-2}.

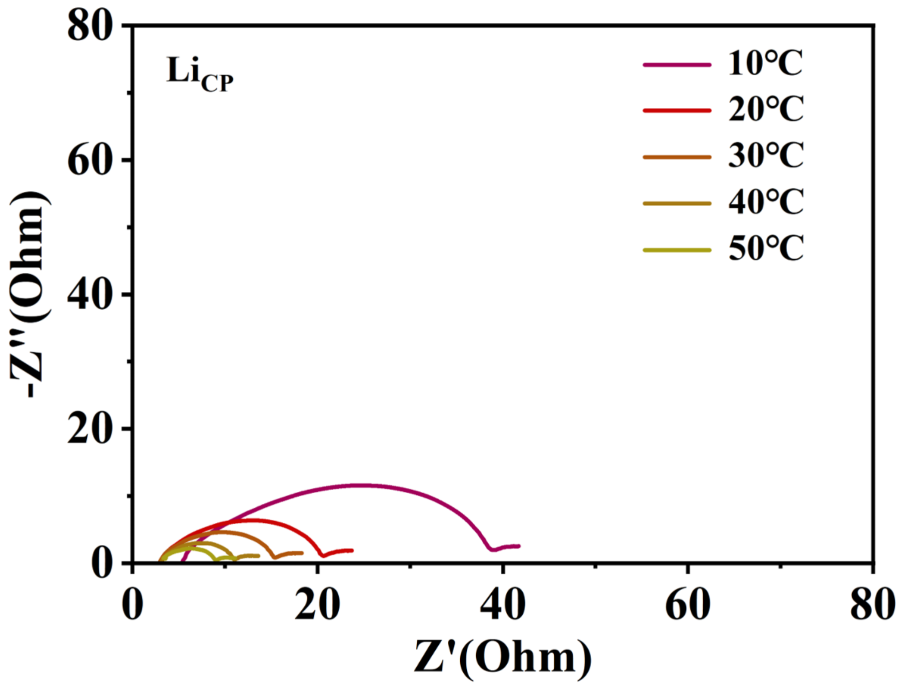

Supplementary Fig. 25 EIS curve for Li$_{CP}$ / Li$_{CP}$. It was measured at different temperatures and shows in five lines.

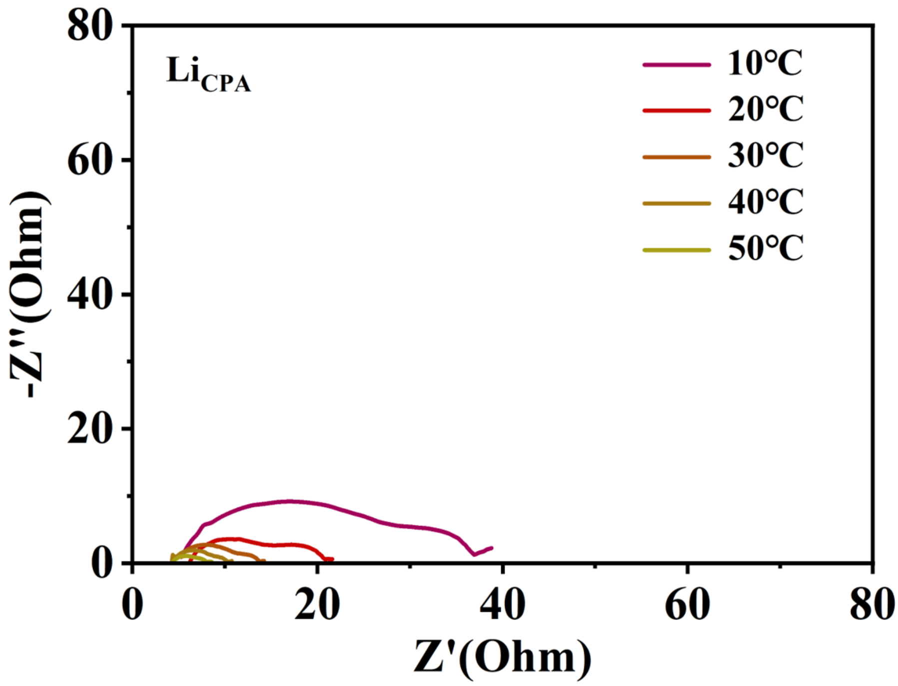

Supplementary Fig. 26 EIS curve for Li$_{CPA}$ / Li$_{CPA}$. It was measured at different temperatures and shows in five lines.

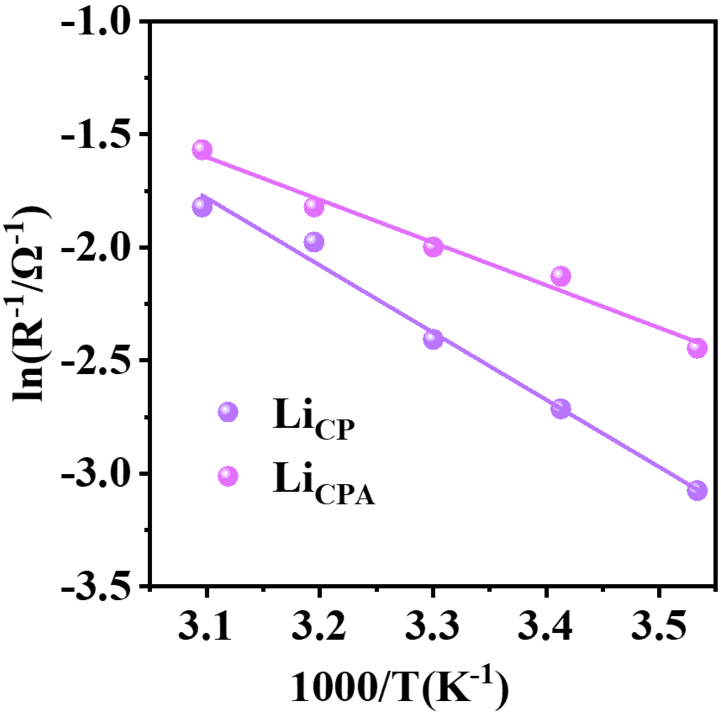

Supplementary Fig. 27 Straight line fitted by R_{ct} from EIS. Corresponding comparison of activation energies was get from symmetrical battery for Li_{CP} and Li_{CPA}.

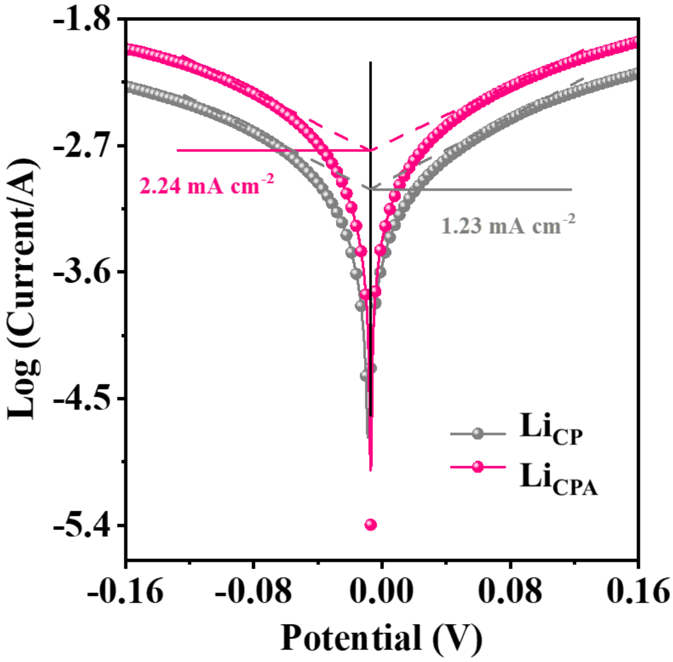

Supplementary Fig. 28 Tafel curve for these two anodes. Tafel slope and exchange current density obtained from this curve of Li/Li battery for Li_{CP} and Li_{CPA}after first cycle

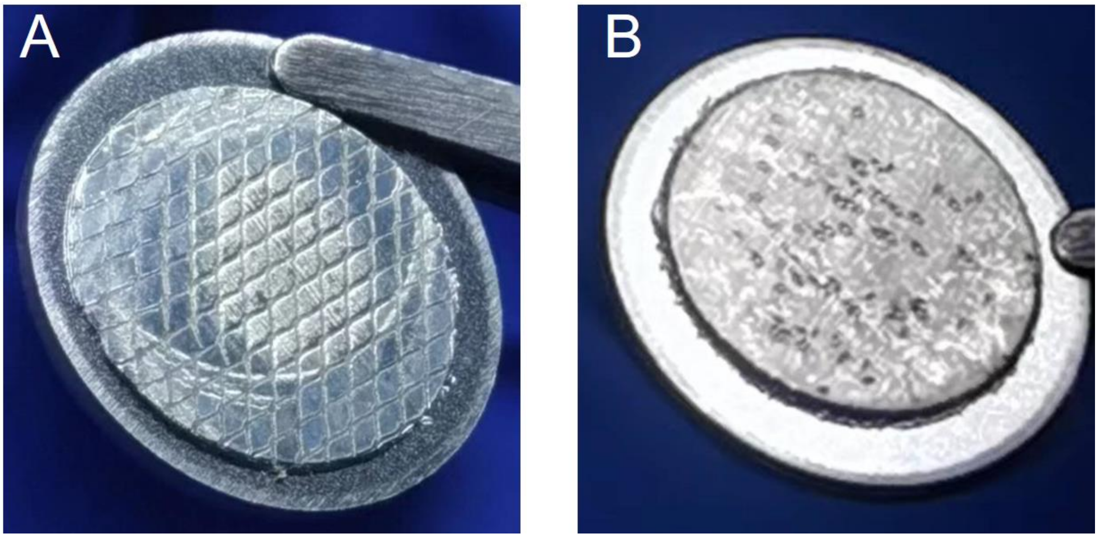

Supplementary Fig. 29 Surface morphology of electrode Li_{EH} (A) and Li_{EL} (B). For, Li_{EH} indentation is prepared through 50 mesh copper mesh, Li_{EL} randomly extrudes 20 pits through tweezers. And diameter of Li_{EH} and Li_{EL} is 12 mm.

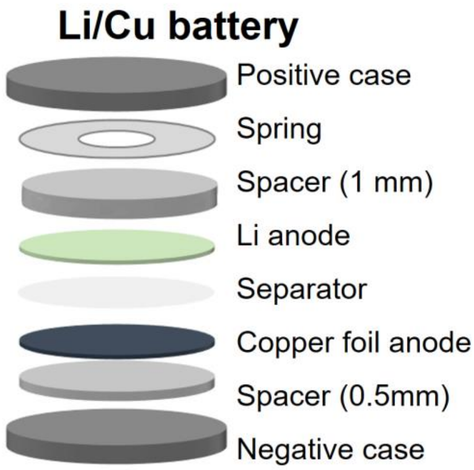

Supplementary Fig. 30 Schematic diagram of the structure of the Li/Cu battery.

Table S1. The parameter used in the model calculation[1, 2].

Model definition	Parameter	Value
Temperature	T	298 K
Barrier height	W	3.75×10^{5}J m^{-3}
Gradient energy coefficient	κ	5×10^{-5}J m^{-1}
Interfacial mobility	L_σ	2.5×10^{-6}m^{3} J^{-1} s^{-1}
Reaction constant	L_η	1.0 s^{-1}
Diffusion coefficient in electrode	D^{Li}	7.5×10^{-13}m^{2}s^{-1}
Diffusion coefficient in solution	D^{s}	7.5×10^{-10}m^{2}s^{-1}
Conductivity in electrode	σ^{Li}	1.0×10^{7}S m^{-1}
Conductivity in solution	σ^{s}	1.0 S m^{-1}
Symmetric factor	α	0.5
Symmetric factor	β	0.5
Mode of the anisotropy	ω	4
Bulk concentration of Li^{+}	c_0	1000 mol m^{-3}

Table S2. SDE calculation method and value of $Li_{0.1M}$, $Li_{0.5M}$, Li_{1M}, Li_{10M}, Li_{CP} and Li_{CPA}.

Sample	Calculation formula	Ln(Ω)
$Li_{0.1M}$	$A_{80}^{11}A_{69}^{19}A_{50}^{17}A_{33}^{14}A_{19}^{17}A_{2}^{2}$	12373.47883
$Li_{0.5M}$	$A_{112}^{6}A_{106}^{23}A_{83}^{42}A_{41}^{29}A_{12}^{11}A_{1}^{1}$	87856.74488
$Li_{1.0M}$	$A_{146}^{3}A_{143}^{26}A_{117}^{46}A_{71}^{33}A_{38}^{37}A_{1}^{1}$	118201.2401
$Li_{10\ M}$	$A_{200}^{1}A_{199}^{11}A_{188}^{51}A_{137}^{78}A_{59}^{55}A_{4}^{4}$	167882.2918
Li_{CP}	$A_{56}^{3}A_{53}^{10}A_{43}^{22}A_{21}^{11}A_{10}^{8}A_{2}^{2}$	443072.8123
Li_{CPA}	$A_{189}^{1}A_{188}^{36}A_{152}^{115}A_{37}^{23}A_{14}^{14}$	661276.8718

In combination with the statistical data of grain distribution of six samples given by the grain distribution histogram Supplementary Fig. 7, S22 and the scale given by the SEM image Fig. 3a-3d, 5b, 5c. $Li_{0.1M}$, $Li_{0.5M}$, Li_{1M} and Li_{10M} scale length is 20um, 1mm^2 contains 94.84 SEM image area, Li_{EL} and Li_{EH} scale length is 8um, 1mm^2 contains 813.43 SEM image area and the grains in calculation of ln(Ω) should be considered the magnification of area. All samples operate under the same difference of grayscales between pixels.

Table S3. The R_{ct} results of $Li_{0.1M}$, $Li_{0.5M}$, Li_{1M}, Li_{10M}, Li_{CP} and Li_{CPA} form 10 °C to 50 °C.

Sample	10 °C	20 °C	30 °C	40 °C	50 °C
$Li_{0.1M}$	63.48Ω	35.77Ω	25.35Ω	16.44Ω	9.18Ω
$Li_{0.5M}$	44.66Ω	30.03Ω	20.59Ω	11.86Ω	8.10Ω
$Li_{1.0M}$	37.25Ω	23.14Ω	15.66Ω	10.52Ω	7.27Ω
Li_{10M}	32.01Ω	17.78Ω	12.91Ω	8.23Ω	6.42Ω
Li_{CP}	21.66Ω	15.09Ω	11.10Ω	7.22Ω	6.18Ω
Li_{CPA}	11.54Ω	8.40Ω	7.38Ω	6.17Ω	4.80Ω

Table S4. Performance comparison with previous work.

Thickness of anode	Test rate	Cycles	Ref
50 [um]	0.2 C	200	3
50 [um]	0.5 C	300	4
50 [um]	1 C	300	5
100 [um]	1 C	360	6
400 [um]	1 C	200	7
24.4 [um]	3 C	800	This work

Table S5. Sample statistics for event and ROP of Li_{EL} and Li_{EH}

Event group	FC	ROP
Li_{EL}	31 32 34	2.01
Li_{EH}	67 68 72	2.58

Reference

1. Hong Z, Viswanathan V. Prospect of Thermal Shock Induced Healing of Lithium Dendrite. *ACS Energy Lett* **4**, 1012-1019 (2019).
2. Chen L*, et al*. Modulation of dendritic patterns during electrodeposition: A nonlinear phase-field model. *J Power Sources* **300**, 376-385 (2015).